

Terahertz magnetoconductivity of excitons and electrons in quantum cascade structures

J. Lloyd-Hughes,^{1,*} H. E. Beere,² D. A. Ritchie,² and M. B. Johnston^{1,†}

¹*Department of Physics, Clarendon Laboratory, University of Oxford, Parks Road, Oxford OX1 3PU, United Kingdom*

²*Department of Physics, Cavendish Laboratory, University of Cambridge, Madingley Road, Cambridge CB3 0HE, United Kingdom*

(Received 28 November 2007; revised manuscript received 21 January 2008; published 18 March 2008)

We examined the quasiparticles formed by the photoexcitation of GaAs/AlGaAs terahertz quantum cascade structures using terahertz time-domain spectroscopy. At low temperature and excitation density the measured conductivity was excitonic, with a $1s$ - $2p$ transition energy indicative of three-dimensional excitons correlated across the quantum well barriers. Free electrons increasingly dominated the conductive response at higher lattice temperatures and excitation densities. Under an external magnetic field transitions from the $1s$ level into $2p$ states with different magnetic quantum number were observed, while at high excitation densities the electron cyclotron resonance became more prominent.

DOI: [10.1103/PhysRevB.77.125322](https://doi.org/10.1103/PhysRevB.77.125322)

PACS number(s): 73.21.-b, 71.35.Ji, 71.70.Di, 78.47.J-

I. INTRODUCTION

In semiconductor nanostructures quantum confinement can create novel materials with tailorable optical and electronic properties substantially different from bulk systems.^{1,2} For instance, quantum cascade heterostructures can be used to make lasers and photodetectors at mid- and far-infrared wavelengths.³⁻⁵ Recent work on terahertz quantum cascade lasers has focused upon covering the spectral range below 2 THz,⁶ measuring their single- and multipass gain,⁷ and enhancing their output power, including by applying a strong magnetic field perpendicular to the wells.^{8,9} In-plane carrier confinement may be required to create terahertz quantum cascade lasers that operate closer to room temperature, and applying a magnetic field is a straightforward way to investigate this. It is therefore highly desirable to investigate the properties of quasiparticles confined quantum mechanically and magnetically in quantum cascade structures, from the viewpoint of both fundamental and applied semiconductor physics.

Quantum confinement can promote the formation of excitons—bound electron-hole pairs—which often dominate the optoelectronic behavior of semiconductor nanostructures.² Unconfined (three-dimensional) excitons have a binding energy of $E_n = R_X/n^2$, where $n=1, 2, 3, \dots$ and the Rydberg constant is $R_X = 4.2$ meV for GaAs.¹⁰ Quasi-2D excitons can be created within semiconductor quantum wells, with narrow wells and high barriers enhancing the confinement and thus the exciton binding energy.² For 2D excitons, the binding energy is $E_m = R_X/(m+1/2)^2$ (where $m=0, 1, 2, \dots$), i.e., the ground state is more strongly bound than in 3D. Dipole allowed electromagnetic transitions can occur between different excitonic levels, with energies typically in the terahertz (far-infrared) frequency range in III-V semiconductors. While interband emission and absorption processes are altered by the presence of excitons, only low momentum states can be accessed optically, and coherent polarization effects can lead to photoluminescence at the excitonic resonances even without a population of excitons.¹¹ In contrast, the absorption of terahertz radiation promotes transitions between excitons in all momentum states, as has been demonstrated for excitons in GaAs quantum wells^{12,13} and in bulk Cu_2O .¹⁴

In this article we report the magnetoconductivity of excitons and electrons in quantum cascade structures, which we have measured using terahertz time-domain spectroscopy. We used near-infrared pulses to generate a quasiparticle distribution, and determined the complex conductivity using broadband pulses of terahertz radiation. At low excitation densities the observed response was dominated by the $1s$ - $2p$ exciton transition at 5.0 meV, demonstrating that excitons are partially confined and that electron-hole correlations persist across the superlattice structure. At higher quasiparticle densities the photoresponse was increasingly indicative of an electron-hole plasma. Under an applied magnetic field the excitonic $1s$ - $2p$ transition was witnessed to split into two states, resulting from the lifting of the degeneracy of the $2p$ energy level. The electron cyclotron resonance was observed at high photoexcitation fluences.

II. EXPERIMENTAL METHOD

Quantum cascade samples were mounted in the variable temperature insert of a split-coil superconducting magnet. The transmission of single-cycle pulses of terahertz radiation through the cascade samples was determined using a terahertz time-domain spectroscopy setup similar to that described in Ref. 15. The Ti:sapphire laser system used produced 100 fs duration pulses of energy 11 nJ, at 800 nm wavelength, and with a repetition rate of 80 MHz. A schematic of the sample geometry is shown in the inset to Fig. 1, where the terahertz beam path is labeled “THz.” The terahertz pulses were TE-polarized, parallel to the plane of the quantum wells, making intersubband transitions dipole forbidden.

Photoexcitation of the sample was at 800 nm, with the pump beam (labeled “IR”) at right angles to the terahertz beam. A magnetic field from $B=0$ –6.5 T was applied along the terahertz beam path. The pump beam was optically chopped, and the photoinduced change in the transmitted terahertz pulse was measured via a lock-in amplifier referenced to the chopper, by scanning the terahertz delay. The complex conductivity $\sigma(\omega)$ of the photoexcited region was calculated from the measured transmission change, at sample angles of $\theta=30^\circ$ and 45° (Fig. 1). This was performed at

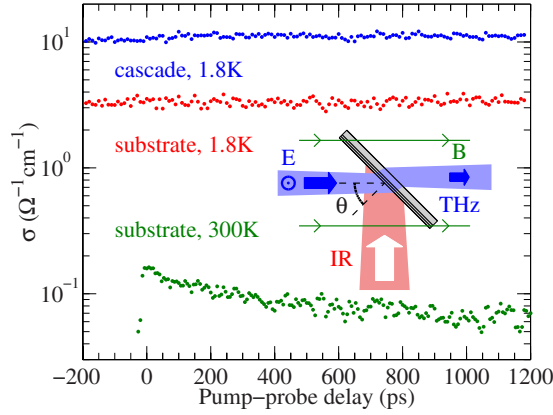


FIG. 1. (Color online) Time-resolved photoexcited conductivity $|\sigma|$ of the 2.0 THz quantum cascade structure vs pump-probe delay time, averaged over the bandwidth of the terahertz pulse and at zero magnetic field. Data are shown obtained on photoexciting the cascade structure at 1.8 K (top points), the substrate at 1.8 K (middle), and the substrate at 300 K (bottom). The experimental geometry is shown in the inset, as described in the text.

various delay times of the pump beam. Additionally, the conductivity of the semi-insulating GaAs substrate data was obtained by rotating the sample to $\theta=225^\circ$. The photoexcited conductivity of the cascade structure was determined at various sample temperatures T , pump fluences F , and applied magnetic field strengths B .

The quantum cascade structures examined in this study have been shown to lase at 2.0 THz and 2.9 THz, and are described fully in Refs. 16 and 17. No postgrowth processing of the as-grown wafers was performed. Both designs had bound-to-continuum laser transitions, and an average GaAs quantum well thickness of about 13 nm. The $\text{Al}_x\text{Ga}_{1-x}\text{As}$ barriers were between 1 nm and 4 nm thick, and $x=0.1$ ($x=0.15$) for the 2.0 THz (2.9 THz) sample. The total thickness of the ~ 100 repeat units of the active region was $\geq 10 \mu\text{m}$, far exceeding the penetration depth ($\sim 1 \mu\text{m}$) of GaAs at 800 nm. A 70 nm thick n -doped layer was present on top of the sample. The photoexcited conductivity response was therefore dominated by the quasiparticles generated within the cascade heterostructure.

III. RESULTS

A. Dynamics of the photoconductivity

The time-resolved conductivity of the 2.0 THz cascade structure was obtained by monitoring the photoinduced change in the peak of the terahertz electric field transmitted through the sample at different pump beam delays t . This corresponds to the conductivity of photoexcited carriers averaged over the frequencies in the terahertz probe pulse.¹⁸ In Fig. 1 the photoconductivity of the cascade structure at a temperature of 1.8 K (sample angle $\theta=45^\circ$) is compared with that obtained on photoexcitation of the semi-insulating GaAs substrate ($\theta=225^\circ$) at 1.8 K and 300 K. The “one-dimensional” pump probe scan for the substrate at 300 K is typical of bulk GaAs: The conductivity rapidly rises at zero

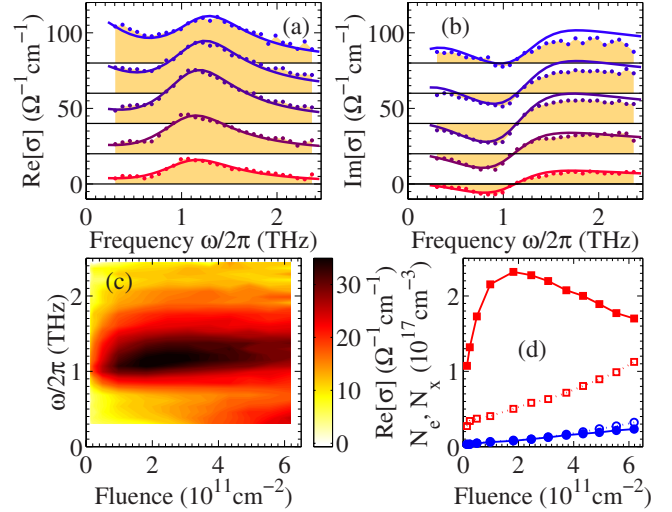


FIG. 2. (Color online) Spectral dependence of the photoexcited conductivity $\sigma(\omega)$ at various pump fluences at $T=1.8$ K. Points and shaded areas show (a) $\text{Re}[\sigma]$ and (b) $\text{Im}[\sigma]$ at pump fluences (from bottom to top) of $0.14, 0.50, 2.5, 3.7,$ and $6.2 \times 10^{11} \text{ cm}^{-2}$ photons per pulse. Solid lines are fits using the conductivity model described in the text. (c) $\text{Re}[\sigma]$ as a function of photon frequency and pump fluence (black equals high conductivity). (d) Extracted exciton density N_x (squares) and electron density N_e (circles) from fits to $\sigma(\omega)$ at various pump fluences, at $T=1.8$ K (filled markers) and $T=20$ K (unfilled markers).

time delay and decays nonexponentially owing to surface recombination.¹⁹ At $T=1.8$ K, however, the lifetime of photoexcited electrons in bulk GaAs becomes substantially longer than the time period between laser pulses (12.5 ns), resulting in nonzero conductivity at negative pump delay times ($t \leq 0$) and no time-dependent response. The long electron lifetime has the additional consequence of enhancing the photoexcited carrier density above that generated by a single pulse, increasing the conductivity. The reduction in carrier-TO phonon scattering at low temperature²⁰ further boosts the conductivity. Considering now the data for the cascade structure at $T=1.8$ K, the conductivity is roughly three times larger than that of bulk GaAs at the same temperature, implying a corresponding enhancement of the mobility. The conductivity at $t \geq 0$ ps is slightly larger than that at $t \leq 0$ ps, and from this a mean recombination lifetime of 144 ns of the photoexcited quasiparticles was calculated. This value is long in comparison to typical lifetimes of excitons in quantum wells (of the order of 100 ps, Ref. 21), and may result from an enhanced electron-hole separation created by the quantum cascade structure.

B. Fluence and temperature dependence of the conductivity

The frequency dependence of the complex conductivity of photocarriers in the cascade samples was determined at a fixed pump-probe time delay ($t=200$ ps, although as shown in Fig. 1 there is essentially no dynamic behavior), and is shown in Fig. 2 at various photoexcitation fluences from 3.4 to $154 \mu\text{J cm}^{-2}$. This corresponds to a photon fluence of $F \sim (0.14-6.2) \times 10^{11} \text{ cm}^{-2}$ per pulse. Looking first at $\sigma(\omega)$

at the lowest pump fluence [lowest points in Figs. 2(a) and 2(b)], it can be seen that the real part of the conductivity peaks at 1.1 THz (4.6 meV), while the imaginary part of the conductivity has a zero crossing at the same frequency. This shape is a characteristic of both excitonic transitions^{12,14,22} and of surface plasmons.²³ However, for surface plasmons the frequency of the resonance increases with the square root of the carrier density. The measured conductivity shows no substantial shift in the resonant frequency with a $40\times$ increase in pump fluence, as the data in Figs. 2(a)–2(c) illustrate, ruling out surface plasmons as the dominant excitation.

The measured $\sigma(\omega)$ at low fluence can be well modeled by the resonant line shape expected for dipole-allowed transitions from the excitonic $1s$ to $2p$ state,²² with a transition energy $E_{1s-2p}=4.6$ meV [solid red lines in Figs. 2(a) and 2(b)]. The value of E_{1s-2p} is substantially closer to the transition energy for 3D Mott-Wannier excitons in GaAs $E_{1s-2p}=3R_X/4=3.2$ meV than the 2D energy $E_{1s-2p}=32R_X/9=14.9$ meV. This implies that the excitons in our quantum cascade structures are substantially 3D, and we therefore utilized 3D hydrogenic wave functions²⁴ in order to calculate the $1s$ - $2p$ oscillator strength and extract N_X from our fits. Similar curves to those in Fig. 2 were obtained for the 2.9 THz cascade structure, indicating that the exciton binding energy is comparable in the two designs. In contrast, previous terahertz time-domain spectroscopy measurements have found $E_{1s-2p}=8.3$ meV for 10 nm GaAs/Al_{0.3}Ga_{0.7}As quantum wells,¹³ and $E_{1s-2p}=7.0$ meV for 14 nm GaAs/Al_{0.3}Ga_{0.7}As quantum wells.^{12,22} For our quantum cascade structures both the superlattice and the low Al barrier height act to reduce the confinement and therefore the exciton binding energy, because the exciton binding energy is lower in Al_xGa_{1-x}As than GaAs (Ref. 25).

The conductivity at higher pump fluence is also shown in Fig. 2. With an increasing fluence we observe (i) the $1s$ - $2p$ transition to shift to higher frequencies, (ii) the peak of the $1s$ - $2p$ transition to rise then fall, and (iii) an increase in the real and imaginary parts of $\sigma(\omega)$ below the $1s$ - $2p$ resonance. We have modeled these changes by adding to the excitonic conductivity the Drude conductivity of a free-electron gas. We obtain the solid curves in Figs. 2(a) and 2(b) using a constant electron scattering rate of 10^{13} s⁻¹ and varying the electron density N_e , exciton density N_X and E_{1s-2p} . A weak increase in E_{1s-2p} with fluence was found, from 4.6 meV to 5.8 meV at the highest fluence, which may result from exciton-exciton interactions renormalizing the exciton self-energy at high densities.²⁶ The obtained carrier densities are plotted in Fig. 2(d) against incident pump fluence. The electron density at $T=1.8$ K (filled circles) increases linearly with fluence F , while the exciton density (filled squares) saturates at $F=2\times 10^{11}$ cm⁻² before reducing at higher fluences. A similar effect was reported in Ref. 22 for single GaAs quantum wells, and was attributed to the exciton population acting like a free electron gas at high densities. Alternatively, the localized heating of the lattice by the pump beam may reduce the exciton density at high fluence via thermal dissociation.

The conductive response was also measured at a lattice temperature of 20 K at varying fluence. The measured conductivity (not shown) exhibited $E_{1s-2p}=5.0$ meV at all flu-

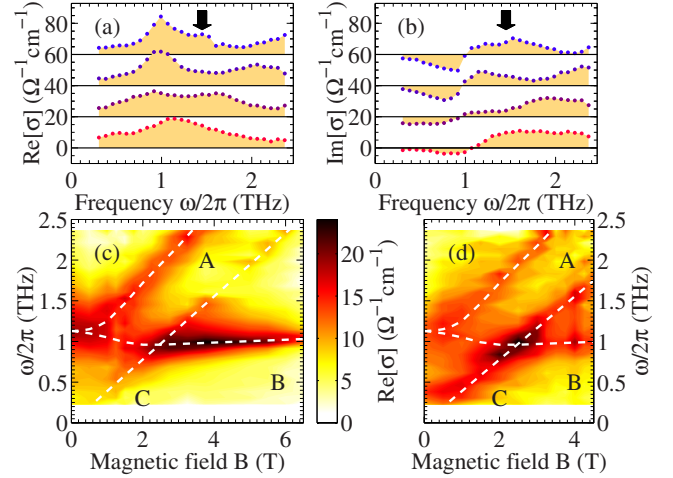


FIG. 3. (Color online) Magnetic field B dependence of the photoexcited conductivity $\sigma(\omega)$ at 1.8 K and sample angles of (a)–(c) 30° and (d) 45° . (a) and (b) plot the real and imaginary parts of the measured $\sigma(\omega)$ at $B=0, 1.75, 2.75,$ and 3.75 T (from bottom to top). (c) At an electron density $N_e=7\times 10^{15}$ cm⁻³ the real part of $\sigma(\omega, B)$ peaks around the dotted lines (guides to the eye), described in the text. (d) At a higher electron density of $N_e=1.2\times 10^{16}$ cm⁻³ the electron cyclotron resonance is more prominent, indicated by the dotted line.

ences, and the exciton density (open squares in Fig. 2) was found to be lower than at $T=1.8$ K. Correspondingly, the electron density at 20 K (open circles) was enhanced. This finding can be explained by the greater thermal dissociation of excitons into electron-hole pairs at higher T .

C. Magnetoconductivity of excitons and electrons

Recent years have seen increased interest in the behavior of quantum cascade lasers under external magnetic fields.^{8,9} Accordingly, we have investigated the response of electrons and excitons in our quantum cascade structures to an external magnetic field B applied parallel to the incident terahertz beam (Fig. 1 inset). In contrast to cyclotron resonance studies performed using narrowband terahertz sources^{27,28} this approach allowed the complex, frequency-dependent conductive response to be determined at each applied magnetic field. Previously, terahertz time-domain spectroscopy has been used to examine cyclotron motion in two-dimensional electron gases^{29,30} and parabolic quantum wells.³¹

Data were obtained at low and high pump fluence for $B=0$ – 6.5 T, and at sample angles of 30° and 45° . In Figs. 3(a) and 3(b) the real and imaginary parts of $\sigma(\omega)$ at $N_e=7\times 10^{15}$ cm⁻³ are plotted at discrete values of B , while the real part of $\sigma(\omega, B)$ is shown in Fig. 3(c). No substantial change in σ with B can be seen up to $B=1.0$ T, above which the $1s$ - $2p$ peak begins to split into two modes, labeled A and B in Fig. 3(c). Mode A increases linearly with field above $B=1.5$ T, while mode B exhibits a weak redshift then a shallow blueshift with B .

Under a magnetic field the electric-dipole-allowed transitions between quasi-2D hydrogenic states conserve parity and obey $\Delta m=\pm 1$, where m is the magnetic quantum

number.³² The two modes can be assigned to dipole-allowed transitions between magnetoexciton states with different magnetic quantum number, namely $1s-2p_+$ for mode *A* and $1s-2p_-$ for mode *B*, where we use 3D spectroscopic notation to describe the excitonic states.³² The $1s-2p_0$ transition is dipole forbidden, as the $2p_0$ level has $m=0$.³² The dispersion of the modes with magnetic field arises from the excitonic wave functions becoming increasingly 2D at high B . Transitions between excitonic states with different electron or hole spin states are not observed here, as the splitting energies are smaller than the transition linewidths.

The observed behavior of the $1s-2p_{\pm}$ modes is in agreement with variational calculations of the energy levels of hydrogenic systems.^{33,34} A detailed calculation of the evolution of the $1s-2p_{\pm}$ matrix elements with B is required in order to extract the magnetoexciton density from the data of Fig. 3. However, the oscillator strength of the $1s-2p_-$ transition (mode *B*) can be seen to decrease at high magnetic field, in agreement with the trend reported in Ref. 33.

An additional resonance in the conductivity is visible for the $B=3.75$ T data in Figs. 3(a) and 3(b), as indicated by the arrows. This mode is the electron cyclotron resonance, as shown by the dotted line labeled *C* in Fig. 3, which runs through $\omega=0$, $B=0$. The gradient of line *C* yields the effective mass of the cyclotron mode as $m_C=(0.073 \pm 0.002)m_e$, typical of conduction band electrons in a GaAs superlattice. In contrast, the effective mass $m_A=(0.061 \pm 0.002)m_e$ of mode *A* at high B corresponds to the reduced effective mass of heavy hole excitons in the superlattice. Taking these values of the exciton and electron effective mass the calculated hole effective mass is $m_h=(0.37 \pm 0.09)m_e$, that of heavy holes in GaAs. It is worth noting that the modes in Figs. 3(c) and 3(d) cannot be described by the magnetoplasmon dispersion relation³¹ because mode *A* does not tend to the cyclotron resonance at large magnetic fields.

The cyclotron resonance is more clearly visible in Fig. 3(d), which shows $\text{Re}[\sigma(\omega, B)]$ obtained at a sample angle of 45° and a higher electron density of $N_e=1.2 \times 10^{16} \text{ cm}^{-3}$ (at $B=0$ T). Modes *A* and *B* are again visible in this figure, and exhibit the same B dispersion as in Fig. 3(c). The similarity between the data obtained at different sample angles further indicates that excitons are quasi-3D in quantum cascade structures since the modes have not changed position, even though the component of B perpendicular to the wells has altered. However, the electron cyclotron resonance (mode *C*) is more pronounced in Fig. 3(d) as a result of the greater proportion of electrons in comparison to excitons, and the $1s-2p_{\pm}$ transitions are correspondingly weaker.

IV. CONCLUSION

In summary, we have measured the terahertz-frequency conductive response of magnetoexcitons and electrons in quantum cascade structures. The excitonic $1s-2p$ transition was observed at zero magnetic field and was characteristic of quasi-3D excitons. Under a magnetic field this excitonic transition split according to the magnetic quantum number of the final state. With increasing field the $1s-2p_+$ energy was strongly enhanced, while the $1s-2p_-$ transition changed less substantially. The effective masses of exciton and electrons in the cascade structure were determined directly from experiment, and the heavy hole mass was inferred. The results presented herein provide valuable information on the fundamental properties of excitons and electrons in quantum cascade structures, knowledge that will aid further improvements of device design and theory.

ACKNOWLEDGMENT

The authors would like to acknowledge financial support from the EPSRC (UK).

*Present address: ETH Zürich, Institute for Quantum Electronics, Wolfgang-Pauli-Strasse 16, 8093 Zürich, Switzerland. james.lloyd-hughes@phys.ethz.ch

†m.johnston@physics.ox.ac.uk

¹G. D. Scholes and G. Rumbles, *Nat. Mater.* **5**, 683 (2006).

²P. Bhattacharya, *Properties of III-V Quantum Wells and Superlattices* (IEEE, New York, 1996), Chap. 2, pp. 33–94.

³R. Köhler, A. Tredicucci, F. Beltram, H. Beere, E. Linfield, A. Davies, D. Ritchie, R. Iotti, and F. Rossi, *Nature (London)* **417**, 156 (2002).

⁴M. Graf, G. Scalari, D. Hofstetter, J. Faist, H. Beere, E. Linfield, D. Ritchie, and G. Davies, *Appl. Phys. Lett.* **84**, 475 (2004).

⁵J. Faist, F. Capasso, D. Sivco, C. Sirtori, A. Hutchinson, and A. Cho, *Science* **264**, 553 (1994).

⁶C. Walther, G. Scalari, J. Faist, H. Beere, and D. Ritchie, *Appl. Phys. Lett.* **89**, 231121 (2006).

⁷J. Kröll, S. S. Dhillon, X. Marcadet, M. Calligaro, C. Sirtori, and K. Unterrainer, *Nature (London)* **449**, 698 (2007).

⁸V. Tamosiunas, R. Zobl, J. Ulrich, K. Unterrainer, R. Colombelli,

C. Gmachl, K. West, L. Pfeiffer, and F. Capasso, *Appl. Phys. Lett.* **83**, 3873 (2003).

⁹G. Scalari, S. Blaser, J. Faist, H. Beere, E. Linfield, D. Ritchie, and G. Davies, *Phys. Rev. Lett.* **93**, 237403 (2004).

¹⁰D. D. Sell, *Phys. Rev. B* **6**, 3750 (1972).

¹¹S. W. Koch, M. Kira, G. Khitrova, and H. M. Gibbs, *Nat. Mater.* **5**, 523 (2006).

¹²R. A. Kaindl, M. A. Carnahan, D. Hagele, R. Lovenich, and D. S. Chemla, *Nature (London)* **423**, 734 (2003).

¹³R. H. M. Groeneveld and D. Grischkowsky, *J. Opt. Soc. Am. B* **11**, 2502 (1994).

¹⁴R. Huber, B. A. Schmid, Y. R. Shen, D. S. Chemla, and R. A. Kaindl, *Phys. Rev. Lett.* **96**, 017402 (2006).

¹⁵M. B. Johnston, L. M. Herz, A. L. T. Khan, A. Köhler, A. G. Davies, and E. H. Linfield, *Chem. Phys. Lett.* **377**, 256 (2003).

¹⁶C. Worrall, J. Alton, M. Houghton, S. Barbieri, H. E. Beere, D. Ritchie, and C. Sirtori, *Opt. Express* **14**, 171 (2006).

¹⁷S. Barbieri, J. Alton, H. E. Beere, J. Fowler, E. H. Linfield, and D. A. Ritchie, *Appl. Phys. Lett.* **85**, 1674 (2004).

- ¹⁸This approach is only valid if the arrival time of the terahertz pulse does not change substantially with pump delay, a condition that we verified experimentally.
- ¹⁹J. Lloyd-Hughes, S. K. E. Merchant, F. Lan, H. H. Tan, C. Jagadish, E. Castro-Camus, and M. B. Johnston, *Appl. Phys. Lett.* **89**, 232102 (2006).
- ²⁰P. Y. Yu and M. Cardona, *Fundamentals of Semiconductors*, 3rd ed. (Springer, New York, 2003).
- ²¹J. Martinez-Pastor, A. Vinattieri, L. Carraresi, M. Colocci, P. Roussignol, and G. Weimann, *Phys. Rev. B* **47**, 10456 (1993).
- ²²R. Huber, R. A. Kaindl, B. A. Schmid, and D. S. Chemla, *Phys. Rev. B* **72**, 161314(R) (2005).
- ²³P. Parkinson, J. Lloyd-Hughes, Q. Gao, H. H. Tan, C. Jagadish, M. B. Johnston, and L. M. Herz, *Nano Lett.* **7**, 2162 (2007).
- ²⁴H. Haug and S. Koch, *Quantum Theory of the Optical and Electronic Properties of Semiconductors* (World Scientific, Singapore, 2004), Chap. 10, pp. 163–192.
- ²⁵P. J. Pearah, W. T. Masselink, J. Klem, T. Henderson, H. Morkoc, C. W. Litton, and D. C. Reynolds, *Phys. Rev. B* **32**, 3857 (1985).
- ²⁶N. Peyghambarian, H. M. Gibbs, J. L. Jewell, A. Antonetti, A. Migus, D. Hulin, and A. Mysyrowicz, *Phys. Rev. Lett.* **53**, 2433 (1984).
- ²⁷D. C. Larrabee *et al.*, *Opt. Lett.* **29**, 122 (2004).
- ²⁸J. Cerne, J. Kono, M. S. Sherwin, M. Sundaram, A. C. Gossard, and G. E. W. Bauer, *Phys. Rev. Lett.* **77**, 1131 (1996).
- ²⁹D. Some and A. V. Nurmikko, *Appl. Phys. Lett.* **65**, 3377 (1994).
- ³⁰X. F. Wang, D. J. Hilton, L. Ren, D. M. Mittleman, J. Kono, and J. L. Reno, *Opt. Lett.* **32**, 1845 (2007).
- ³¹R. Zobl, K. Unterrainer, G. Strasser, and E. Gornik, *Semicond. Sci. Technol.* **15**, 315 (2000).
- ³²J. P. Cheng and B. D. McCombe, *Phys. Rev. B* **42**, 7626 (1990).
- ³³C. Aldrich and R. L. Greene, *Phys. Status Solidi B* **93**, 343 (1979).
- ³⁴N. C. Jarosik, B. D. McCombe, B. V. Shanabrook, J. Comas, J. Ralston, and G. Wicks, *Phys. Rev. Lett.* **54**, 1283 (1985).